Int. J. Electrochem. Sci., 16 **(2021)** Article ID: 210838, doi: 10.20964/2021.08.09

International Journal of
ELECTROCHEMICAL
SCIENCE
www.electrochemsci.org

Zinc Ferrite Nanostructure/Multi-Walled Carbon Nanotubes (ZFO/MWCNTs) Nanocomposite as Sensor for Homovanillic Acid Detection in Urine Samples for Cancer Therapy Monitoring

Khulood Abu Al-Ola[1], *Alia Abdulaziz Alfi*[2], *Ahmed Hameed*[2], *Alaa M. Munshi*[2], *Zehba A. Al-Ahmed*[3], *Ali A. Keshk*[4], *Mohamed E. Khalifa*[5], *Nashwa M. El-Metwaly*[2,6*]

[1] Department of Chemistry, College of Science, Taibah University, Saudi Arabia
[2] Department of Chemistry, Faculty of applied science, Umm-Al-Qura University, Makkah, Saudi-Arabia
[3] College of art and science, Dhahran Aljounb, King Khalid University, Saudi Arabia
[4] Depertment of Chemistry, Faculty of Science, Tabuk University, Tabuk-71491, Saudi Arabia
[5] Department of Chemistry, Collage of Science, Taif University, P.O. Box 11099, Taif 21944, Saudi Arabia
[6] Department of Chemistry, Faculty of Science, Mansoura University, El-Gomhoria Street, Egypt
E-mail: XX-ZZ

Received: 9 April 2021 / *Accepted:* 18 May 2021 / *Published:* 30 June 2021

The present work describes a novel electrochemical sensor based on the combination of zinc ferrite nanostructure/multi-walled carbon nanotubes (ZFO/MWCNTs) for sensitive voltammetric determination of homovanillic acid (HVA) in urine samples for diagnosis of neuroblastoma. Different ferrite nanostructures doped with Zn, Cu or Mn, were synthesized and characterized with XRD, SEM, TEM and, FTIR. ZFO/MWCNTs nanocomposite showed an excellent electrocatalytic activity towards the oxidation of HVA with a linear response in the concentration range from 0.415 to 3.225×10^{-6} mol L^{-1} and the detection limit of 0.148×10^{-6} mol L^{-1}. The high resolution between the HVA voltammetric peak and those for uric acid, ascorbic acid, and dopamine introduced the fabricated sensors as an efficient analytical tool for submicromolar voltammetric determination of homovanillic acid in urine samples without prior pretreatment or pre-concentration step. Moreover, the electrode reaction mechanism was studied electrically and correlated with the molecular orbital calculations.

Keywords: Neuroblastoma diagnosis; Homovanillic acid; Ferrite nanocomposite; Differential pulse voltammetry; Urine analysis; Molecular orbital calculations.

1. INTRODUCTION

Neuroblastoma is derived from the primordial neural crest which is frequently diagnosed in infancy [1-3]. Neuroblastoma has a wide range of symptoms and arises from primitive sympathetic ganglion cells [4]. Monitoring of the end products of catecholamine metabolism, homovanillic acid (HVA), and vanillylmandelic acid (VMA), in urine samples, represents a promising screening test for neuroblastoma [3] as the abnormally high concentrations can signalize neuroblastoma-like tumors [5], pheochromocytoma [6, 7] and carcinoid [7]. Moreover, early diagnosis of Menkes disease can be performed through assaying of the HVA to VMA ratio in newborn urine samples [8, 9].

Sensitive and selective analytical techniques were reported for the assaying of catecholamines and their metabolites [10]. HPLC methods with electrochemical detection are the most commonly used [11-13]. Gas chromatography (GC) [14, 15], thin layer chromatography [16], high performance thin film chromatography (HPTLC) [17], immunochemical methods [18, 19], spectrophotometric [20] and capillary electrophoretic [5, 21, 22] were also found in literature.

Early diagnosis of cancer can extremely increase the successful treatment of disease; therefore, the screening tools can be an essential approach in this process [23]. Reliable, accurate, and fast results are crucial pre-requisite for the diagnosis of cancer biomarkers. However, the aforementioned separation and spectrometric methods are usually instrumentally complicated, and time-consuming. These disadvantages encouraged the application of electrochemical tools as sensitive, selective, and yet faster, easier, and cheaper to purchase operating costs. Electroanalytical approaches were reported as effective tools for the determination of many organic, pharmaceutical, and biologically active compounds with the possibility of sensor miniaturization and suitability for real-time monitoring [24-27]. Nowadays, a number of well-established clinical analyzers were based on electrochemical principles.

Barek group [28] recently reviewed the electrochemical approaches for the detection of catecholamine metabolites including homovanillic and vanillylmandelic acid. Unmodified glassy carbon [13], carbon fiber [30], carbon paste [31-34], and more recently screen-printed sensors [35, 36] were reported for voltammetric assay of HVA. The major drawback of unmodified voltammetric sensors is their limited selectivity which is usually based on the redox potential of the present species analyte and the electroactive function groups. In such cases, it is difficult to recognize or distinguish redox-active species with similar functional groups or those producing signals at nearby potentials. Modified or tailor-made sensors were reported for improvement of the selectivity and selectivity of the analytical approach. Different modifiers were introduced for voltammetric evaluation of different either cationic or anionic catecholamine metabolites including carbonaceous nanocomposites [37, 38], organic dyes [39, 40], Troeger's Base [41], L-leucine [42], or surfactant [43].

Sol-gel chemical methods offer promising futures to deal with the most drawbacks of the conventional way for the synthesis of mixed oxide minerals in terms of cost-effective and simplicity of preparation. These procedures are based on the preparation of the required oxide salts colloidal suspension solution, which transformed into a gel by dehydration. The resulted gel is calcined to yield the desired oxide nanostructure. Sol-gel was suggested for the synthesis of ferrite nanoparticles of uniform narrow size and modifications opportunity with desired structures with explored areas of its applications [44-47].

Herein, differential pulse voltammetric (DPV) determination of homovanillic acid employing newly synthesized ferrite nanocomposites as electrode modifiers was described. Improved sensitivity with a detection limit below the HVA concentration in the biological samples allows successful application of the proposed sensor for HVA monitoring and early detection of cancer.

2. EXPERIMENTAL

2.1. Reagents and chemicals

Traditional synthetic carbon powders (1-2 µm, Aldrich) and paraffin oil (PO, Merk) were applied for the preparation of the carbon paste electrode. HVA aqueous solution with 1×10^{-4} mol L^{-1} concentration was prepared by dissolving the required homovanillic acid (99%, Sigma-Aldrich) in water. The starting materials were of analytical grade namely; ferric nitrate ($Fe(NO_3)_3$. $9H_2O$, Sigma), manganese nitrate ($Mn(NO_3)_2\cdot 4H_2O$, Sigma), copper nitrate ($Cu(NO_3)_2\cdot 3H_2O$, Sigma), zinc nitrate ($Zn(NO_3)_2$. $6H_2O$, Sigma), citric acid and ammonia solution (Merck). Multiwall carbon nanotubes (MWCNTs, Sigma) were used for the synthesis of the composite. Britton – Robinson buffer was prepared in a usual and the desired pH value was adjusted with the appropriate amount of 2×10^{-1} mol L^{-1} sodium hydroxide solution.

2.2. Synthesis of ferrite nanostructures

A simple and low-cost sol-gel method has been applied for the synthesis of the spinel ferrite NPs at the nominal composition ($Zn_{0.95}$ $M_{0.05}$ Fe_2O_4 (M = Cu, Mn) [44-47]. Models thru co-precipitation process, Zn, Cu, Mn, and Fe nitrates were involved at definite stoichiometric amounts and separately dissolved in the 10 mL distilled water with continuous magnetic starrier at 80 ^oC for 1h. Subsequently, citric acid was added (1:1 ratio to the metal), followed by 10 mL ethylene glycol as polymerization agent, and to instigate the formation of a uniform gel. The as-synthesized uniform gel was autoclaved at 300 ^oC for 5 h in a 50 mL Teflon-lined autoclave. The formed ferrite nanostructures were collected by cooling down to room temperature and washed with ethanol and deionized water repeatedly. The formed precipitates (nominated as ZFO for zinc ferrite, ZCFO for zinc copper ferrite, ZMFO for zinc manganese ferrite, and FO for native ferrite) were dried at 105 °C for 3 h and crushed to get ferrite NPs.

2.3. Apparatus and electrodes

Metrohm voltammetric analyzer (797 VA, Metrohm Switzerland) was used for electrochemical measurements. Measuring cell composed of nanomaterials functionalized carbon paste electrode, Ag/AgCl/KCl (3.0 mol L^{-1} KCl) double-junction reference electrode and wire of platinum auxiliary electrode was used. Analysis of X-ray diffraction studies was measured using X- Shimadzu XRD-6000 ray diffractometer with the incident radiation in the 2θ range from 10° to 80° applying Cu Kα (1.54 Å). ZEISS, EVO-MA10 scanning electron microscope (SEM), and JEOL transmission electron microscope (TEM) were used for the investigation of the morphology. The chemical functional groups corresponding to the synthesized ferrite NPs were detected in the spectrum ranging from 400 to 4000 cm^{-1} with a Shimadzu FT-IR 4200 Infra-Red spectrometer.

The working carbon paste electrodes were fabricated by the intimate blending of 0.2 g of graphite powder and 80 µL paraffin oil, and the resultant homogenous pastes were packed into Teflon piston holders [48]. The electrode surface was modified by three successive drop-casting of 10.0 µL of the nanocomposite suspension (2 mg Zn ferrite and 2 mg MWCNTs in 1.0 mL^{-1} in DMF, Fluka) on the up-end of the electrode. After complete dryness, the working CPEs were rinsed with double distilled water before measurement.

2.4. Analytical procedures

Aliquots of homovanillic acid solution were added to the measuring cell at the desired pH value and the DP voltammograms were recorded at scan rate 0.05 V s^{-1}, pulse width 100 ms, pulse height (pulls amplitude) 50 mV, and pulse time (voltage step time) 12 ms voltage step 6 mV. Calibration graphs were performed by plotting the peak heights against the HVA concentration. The effective parameters as SD, RSD, LOD, and LOQ were calculated [49] and shown in LOD = 3.3 SD/S, LOQ = 10 SD/S; where SD is the standard deviation of intercept and S is the slope of a linear calibration curve.

2.5. Computation studies

Computational calculations were executed to confirm the proposed HVA oxidation mechanism at the electrode surface. Such calculations were carried out with Gaussian 09 suite programs [50].

3. RESULTS AND DISCUSSION

3.1. Characterization of the ferrite nano structures

XRD analyses were carried out to investigate the crystallinity and the chemical composition of the synthesized ZFO and ZFO substituted with either Cu or Mn cations [$M_{0.05}$ $Zn_{0.95}$ Fe_2O_4; where M = Mn and Cu].

XRD profiles of ZFO, ZCFO, ZMFO, and FO NPs as-resulted are specified in Table S1 and Fig. S1. The obtained XRD results confirmed the cubic system structure of zinc ferrite. The utmost peak intense at the 2θ values of 18.62°, 29.84°, 36.12°, 37.14°, 42.82°, 53.62°, 57.41°, and 63.51° which corresponding to the (111), (220), (311), (222), (400), (422), (511), and (440) reflections, respectively confirmed the presence of cubic spinel phase [44-46].

The morphology of ferrite nanoparticles was presented in **S2**. Spongy structures with irregular pores were formed as a result of the syntheses methodology with combustion at 150 °C, followed by calcination at 300 °C. Most of the gases may be vaporized through these two processes forming the porous spongy structure.

The ferrite nanospheres structural properties were more clearly observed by transmission electron microscopy (Fig. S3). The synthesized ferrite nanospheres showed a large amount of well-dispersed phases. The interplanetary spacing was calculated to be 0.327 nm, which corresponds to the (220) interplanetary spacing of ferrite nanospheres. The inner shape is a happy pattern, in which the diameters of the two planes correspond to the planes (311) and (440), indicating that the ferrite nanosphere has an excellent crystal structure. It is observed that every ferrite nanosphere is in general of sphere-like and possesses a uniform size of 15–28 nm.

Fourier Transform Infrared Spectrometry (FTIR) spectra of zinc-iron samples are shown in Fig. S4. The FTIR method was a useful method for getting info on chemical functional groups equal to the iron complexes. The obtained spectra mainly consist of two major peaks at approximately 542-529 cm^{-1} and 360-365 cm^{-1} confirming the construction of the spinel ferrous structure. The first peak at about 363 cm^{-1} is related to vibration of the octahedral sublattice in the spinel structure, while those at about 535 cm^{-1} are related to the vibration mode of tetrahedral sublattice structure [44-47].

3.2. Electrochemical behavior of HVA

Modification of the electrochemical sensors with different metal oxide doped ferrite nanostructures was reported to improve the selectivity and selectivity of the analytical approach [51-53].To examine the electrocatalytic properties of ferrite nanocomposites towards the electrochemical oxidation of HVA, the cyclic voltammograms of 1.234×10^{-6} mol L^{-1} HVA at the bare CPE and Zn ferrite (ZFO/CPE) modified electrodes were recorded in BR buffer solution at pH =2.0 (Fig. 1). On the bare electrode, homovanillic acid showed an anodic peak at 0.758 V corresponding to the formation of its oxidation product 4-aceto-o-quinone, while the reduction of 3,4-dihydroxyphenylacetic acid (DOPAC) showed a reduction peak at 0.347 V [29, 33]. Upon modification with ferrite nanostructures, comparatively improved peak current with shifting of the peak potential towards the negative direction by about 0.035 V. The improvement of the performance may be explained on the basis of faster electron transfer reaction and the possible interaction between HVA and ferrite nanocomposites compared with the bare carbon paste electrode. Moreover, a small oxidation peak appeared at 0.392 V appeared in consecutive scans corresponding to the oxidation of the formed DOPAC [31, 35]. A higher peak current with better resolution of peaks was achieved applying differential pulse voltammetry (DPV) compared with cyclic voltammetry (CV), therefore DPV will be applied in the following studies.

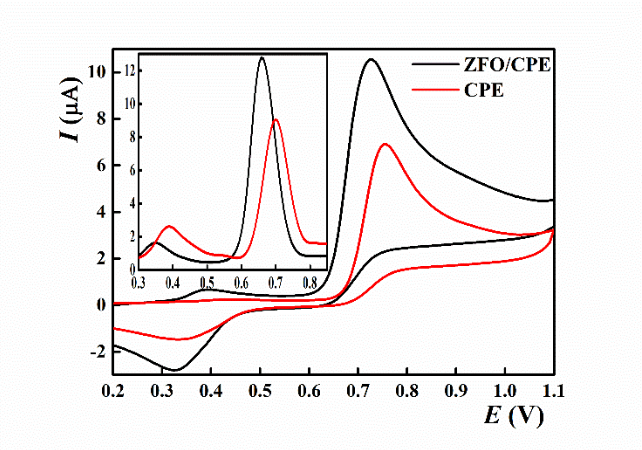

Figure 1. Differential pulse and cyclic voltammograms for 1.234×10^{-6} mol L^{-1} HVA recorded on both blank and Zn ferrite modified carbon paste electrodes in universal Britton–Robinson buffer at pH 2.0 with scan rate 50 mV s^{-1}

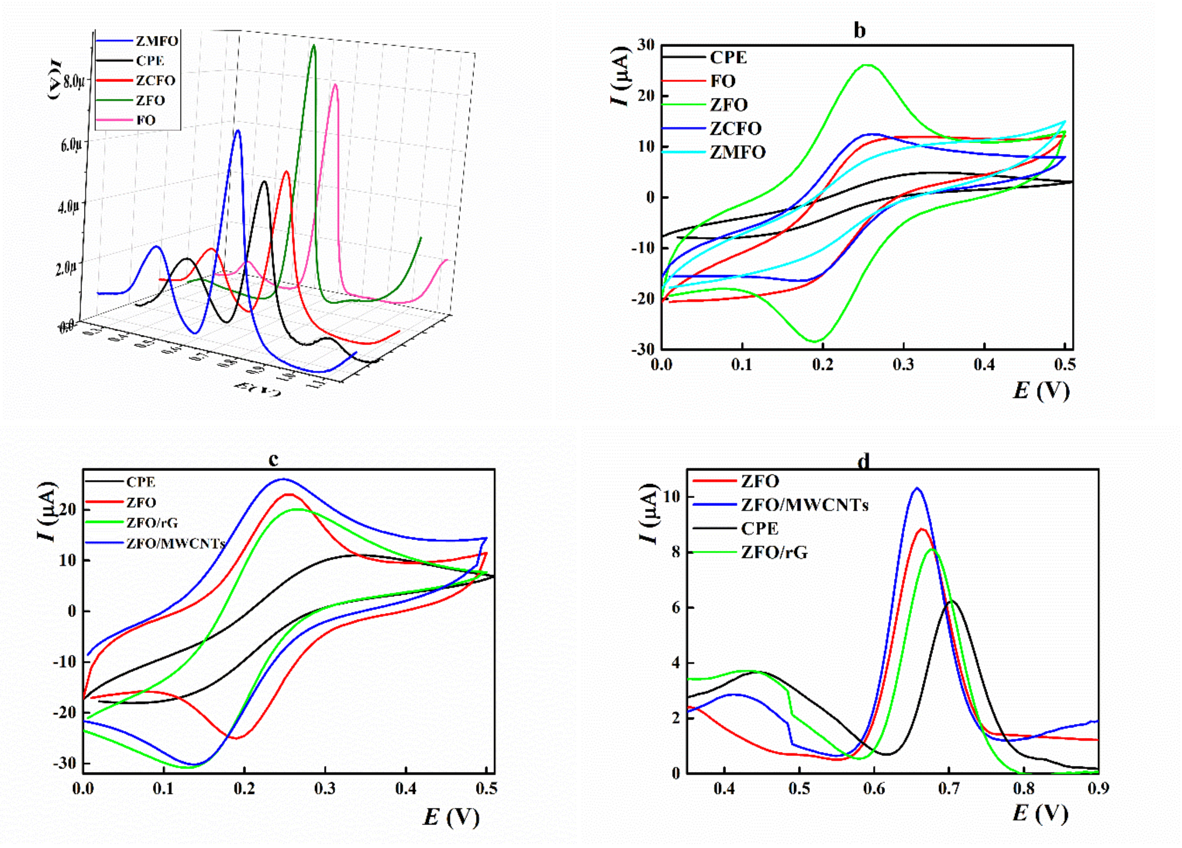

Figure 2. a, d) DPV for 1.234 $\times10^{-6}$ mol L^{-1} HVA using different ferrite nanostructures modified electrodes at pH 2.0; b, c) CV curves of different electrode recorded in 1.0×10^{-3} mol L^{-1} KCl containing 5.0×10^{-3} mol L^{-1} $Fe(CN)_6^{3-/4-}$, scan rate was 50 mV s^{-1}.

Next, the bare working electrodes were modified with different ferrite nanostructures namely; Cu ferrite (ZCFO), Mn ferrite (ZMFO), and Zn ferrite (ZFO) in addition to unmodified ferrite (FO)

(Fig. 2a). Zn ferrite was selected on the basis of improved peak heights and shifting to a more negative potential.

The redox behavior of ferricyanide was investigated over the different ferrite modified electrodes (Fig. 2b, c). In the potential range from 0 to 0.5 with sweep speed 0.05 V s^{-1}, a pair of redox peaks exists on carbon paste electrodes at 0.300 and 0.130 V, which corresponds to the redox reaction of ferricyanide. Upon modification, improved peak currents were achieved (ranged from 3 fold for ZMFO ferrite to about 10 fold for ZFO ferrite compared with bare CPE) and shifting of the peak position to the negative potential direction by about 0.050 V.

Figure 2 c represents the behavior of ferricyanide on ZFO composite with either multiwall carbon nanotubes or graphene nanosheets. The noticeable superior efficiency of ZFO/MWCNTs nanocomposite with well-defined peak and a slight shift of the peak potential were recorded. This can be attributed to the increased effective surface area in the presence of both ZFO nanostructure and MWCNTs which promotes the electron transfer rate.

The electroactive surface area of the modified electrode was explored using $K_3Fe(CN)_6/K_4Fe(CN)_6$ as a probe applying Randles-Sevik equation. The electroactive surface area of the investigated CPE, ZFO/CPE, ZFO/rG/CPE and ZFO/MWCNTs/CPE electrodes were 0.025, 0.238, 0.213 and 0.275 cm^2, respectively [54]. This improved electroactive surface area was reflected in the sensitivity of these sensors towards the target analyte (HVA). As represented in Fig. 2 d, electrodes modified with ZFO/MWNTs showed the highest sensitivity compared with other tested electrodes.

It was reported that HVA oxidation to 4-aceto-o-quinone occurs to give rise to a peak at 0.758 V while the reduction of DOPAC produces a reduction peak at 0.347V (Fig. 1). Successive measurements of 2.0×10^{-6} mol L^{-1} HVA on the same surface resulted in diminishing of the peak height and shifting of the peak position to the more positive potential which may be attributed to the poisoning of the electrode surface by the reaction products [29, 33]. Contrary, modification of the nanocomposite as electrode modifier resists the electrode poisoning and improves the repeatability of the measuring process.

3.3. Optimization of the measuring parameters

3.3.1. Effect of pH

Homovanillic acid showed p*K*a values of 4.35 corresponding to carboxylic group dissociation and 10.34 for the phenolic group [55]. Therefore, the pH of the supporting electrolyte has a major influence on the electrochemical oxidation of HVA. Herein, DPV voltammograms of HVA were recorded on bare and ZFO/MWCNTs/CPE in the pH ranged from 2 to 7 (Fig. 3, S5).

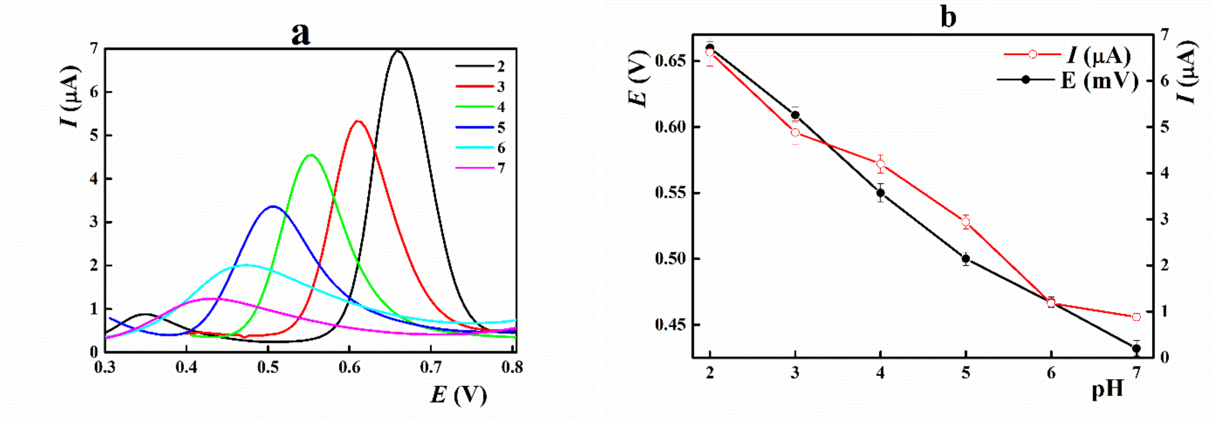

Figure 3. a) Differential pulse voltammograms for 1.234×10^{-6} mol L^{-1} HVA on ZFO/MWCNTs/CPE recorded at different pH values, and b) peak potential and peak current at different pH values.

For carbon paste electrode (S5), shifting the oxidation peak potential to a more positive value with lowering the pH value with the improvement of the peak current is the common feature. Near theoretical Nernstian slope value (E(v)=0.8177 - 0.0545 [pH], r^2=0.9978) was achieved between the peak potential and pH value pH ranged from 5 down to 2, indicating the equal protons and electrons are involved in the redox reactions [56]. At pH higher than the p*K*a value, HVA exists in the anionic form and the oxidation process involves one proton and two electrons [43]. The corresponding slope value was sub-Nernstian (35 mV) indicating unequal protons and electrons involved in the redox reactions. Generally, the highest current response was achieved in the acidic media and the pH 2.

In contrast to carbon paste electrodes, modification with Zn ferrite nanocomposite enhanced the oxidation peak current and maintained the sensitivity over the studied pH range which may be explained on the basis of interaction between HVA molecule and ferrite structure at the electrode surface (Fig. 3). Similar slope values over the pH range from 2 to 7 was obtained (E (v) =0.7441 - 0.0475 [pH], r^2=0.9938).

3.3.2. Effect of the potential sweep rate

Potential scanning rates ranged from 0.020 to 0.18 V s^{-1} were applied on the working electrodes at pH 2 (S 6a). The oxidation peak currents of HVA gradually increase with scan rate and the peak position was shifted towards more positive potentials. The oxidation peak currents were linear against square root of frequency ($I_{(\mu A)}$ =1.3159 + 0.396 [$v^{1/2}$], r^2=0.9905) indicating the typical diffusion control processes at the electrode surface (S 6b). This proposed mechanism was confirmed from the slope value (0.39178) of the linear relationship between the log values of peak current (log (I/μA)) against the log value of the scan rate (log (υ/V s^{-1})) (Fig. S 6c). As showed in S 6d, the oxidation peak potentials were linear with log ν (E (V) = 0.7906 + 0.0395 [log ν], r^2=0.9832). According to Laviron equation, the number of electrons involved in the oxidation process was calculated to be 1.8 [57, 58].

Parallel to carbon paste electrode, the effect of the potential sweep rate on the electrochemical behavior of HVA on Zn ferrite modified electrode was investigated in the range between 0.020 and 0.26 V s^{-1} (Fig. 4a). The peak currents showed high linearity against square root of frequency (r^2=0.98927) sustaining the typical diffusion control processes at the electrode surface (Fig. 4b).

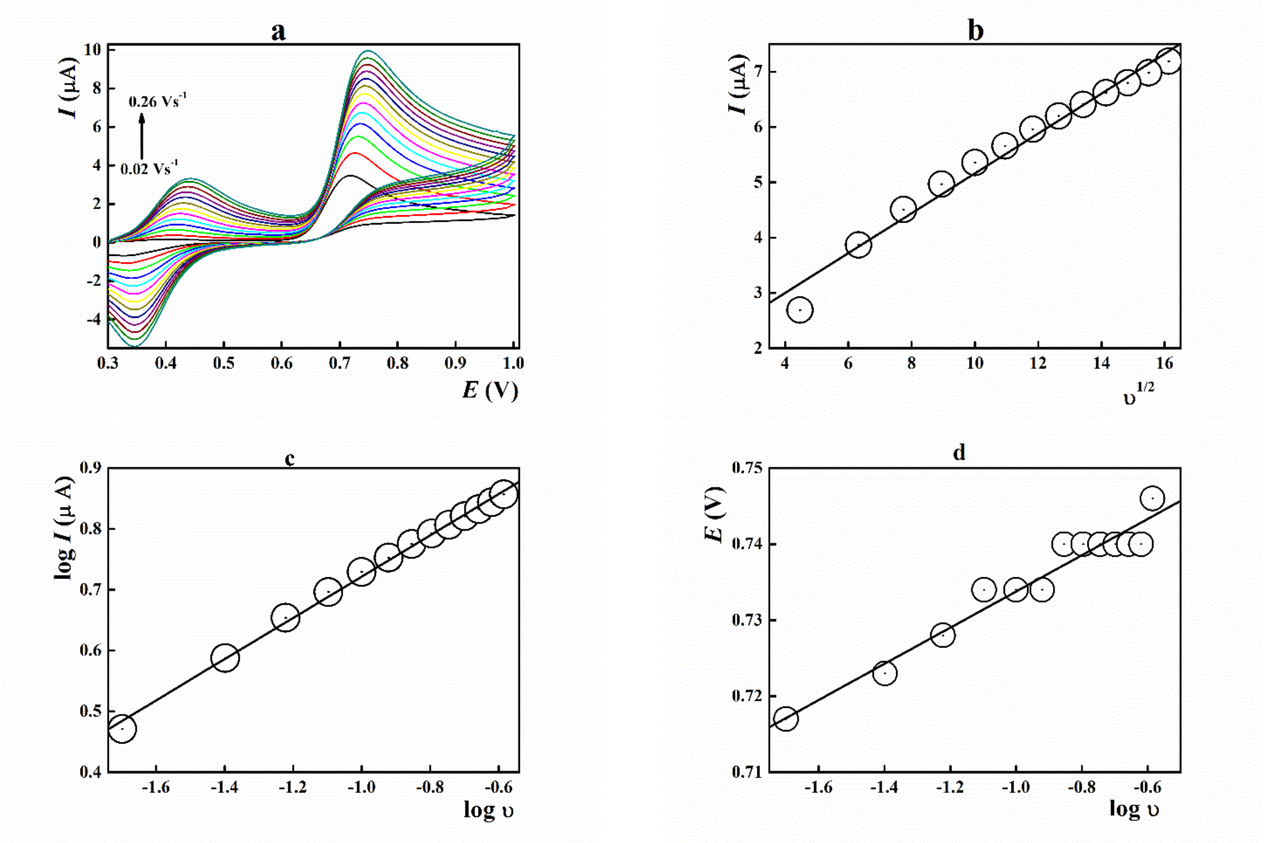

Figure 4. The influence of scan rate on the cyclic voltammetric behavior of 1.23×10^{-6} mol L^{-1} HVA on ZFO/MWCNTs/CPE electrodes at pH 2.

Lower slope value (0.3391) of the linear relation between the log values of peak current (log I) with the log value of the scan rate (log υ) confirm more diffusion of HVA molecule within the nanostructure of Zn ferrite composite which promotes the electron transfer process (Fig. 4c). The oxidation peak potentials of HVA was linear against log ν ($E_{(V)}$ = 0.7576 + 0.0238 [log ν], r=0.9752, Fig. 4d). The number of electrons involved in the reaction process was 2.43 similar to that of blank carbon electrodes.

In conclusion, the electrode reaction process on both electrodes was controlled by diffusion followed by the electron transfer from the diffused HVA at the active edge of the electrode surface generating the oxidation peak. The electrooxidation of the diffused HVA molecule with a precise orientation may be influenced by the interaction of the molecules with the ferrite nanocomposite which reduced the activation energy of the electron transfer by increasing the scan rate.

Eventually, to support the proposed mechanism, Chembio-office-17 program was used for theoretical simulation. Thus the suggested mechanism for the irreversible electrochemical oxidation of the HVA is involving the transfer of 2 electrons and 2 protons as illustrated by molecular orbital calculations (S7 and Table S2) and confirms the effect of the pH and scan rate results (see sec 3.3.1). This suggested mechanism agrees with those postulated in references [42].

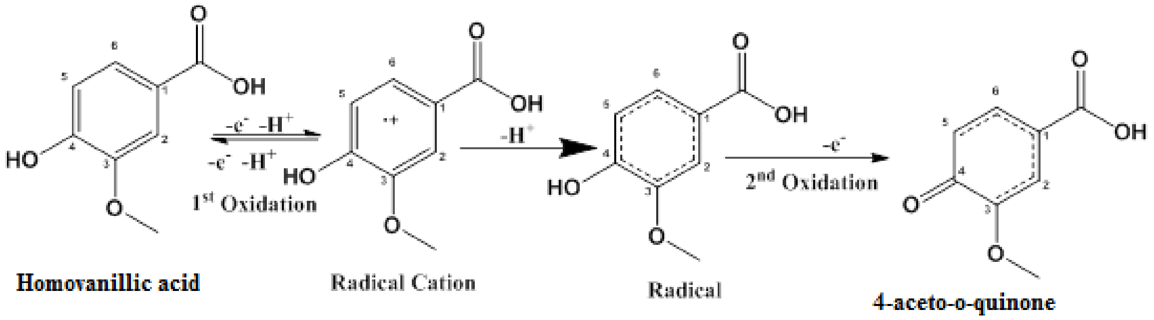

Scheme 1. Postulated oxidation mechanism of HVA at ZFO/MWCNTs/CPE surface

3.4. Analytical characterizations

At the optimum measuring conditions described above, 8-successive additions of homovanillic acid standard solution were added to the measuring cell so that the final concentration ranged from 0.415 to 3.225×10^{-6} mol L^{-1}. For each concentration, differential pulse was recorded, and the subtractive oxidation current from the baseline was calculated and plotted against the corresponding HVA concentration (Fig. 5). Calibration curves showed a high degree of correlation coefficients (I (μA)=6.679±0.146 HVA[molL^{-1}] –(0.174±0.299), r=0.998) with low standard deviations verified the linearity and the applicability of the method over the determined concentration range. The proposed method showed LOD and LOQ values of 0.148×10^{-6} and 0.448×10^{-6}, respectively.

The analytical features of the proposed sensors compared to the previously reported methods were tabulated in Table 1. Simple modification protocols, high measuring repeatability, and fabrication reproducibility with a long operational lifetime can be considered as valuable promising future of the presented sensor. Moreover, the fabricated sensors showed improved sensitivity indicated by lower LOD value compared with those reported in the literature [33, 34, 40, 41, 61- 63].

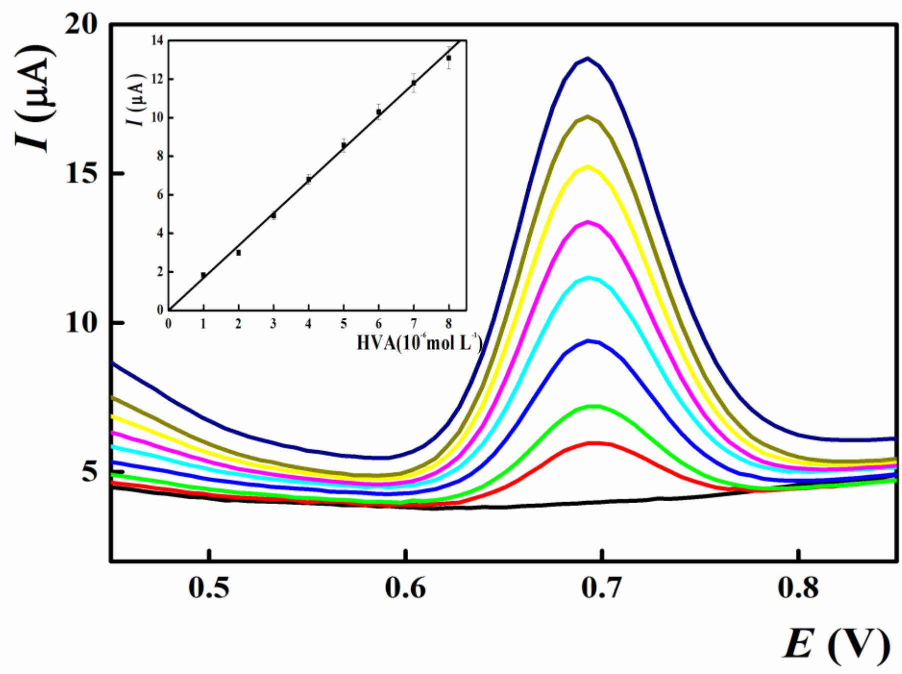

Figure 5. Differential pulse voltammetric determination of HVA using ZFO/MWCNTs/CPE electrode at pH 2.0

Table 1. Modified electrodes for voltammetric determination of homovanilic acid

Modification/working electrode	**Supporting electrolyte**	**Method**	**LOD (×10^{-6} mol L^{-1})**	**Ref.**
Phosphatidylethanolamine/CPE	PB pH 7.4	CV	3.0	33
Carbon paste electrode (CPE)	BR pH 2.0	DPV	0.4	34
Composite carbon film electrode	BR pH 2.0	DPV	0.1	35
Screen-printed electrode	BR pH 3.0	DPV	0.2	36
MWCNTs-Pt/GCE	PB pH 7.0	DPV	0.08	37
Polyvinyl butyral/graphene oxide	PB pH 6.0	DPV	0.18	38
Poly(Alizarin Red S)/GCE	PB pH 3.0	DPV	1.7×10^{-2}	39
Boron doped diamond electrode	PB pH 3.0	DPV	0.6	40
GCE	PB pH 3.0	DPV	0.9	
Nafion/GCE	PB pH 3.0	DPV	0.8	
PNR/GCE	PB pH 3.0	DPV	1.2	
Troeger's/SPE	PB pH 7.0	DPV	2.2	41
L-leucine modified Sol-Gel-Carbon electrode	PB pH 7.4	DPV	0.1	42
Molecularly imprinted polymer/GCE	pH 1.1 with 40% acetonitrile	DPV	7.0×10^{-3}	62
Poly(3-amino-5-mercapto-1,2,4-triazol)/GCE	PB pH 7.2	ChA	9.42×10^{-5}	59
Cu/GCE	PB pH 7.2	SWV	1.0×10^{-2}	60
Boron doped diamond electrode	0.1 mol L^{-1} 1 HCl	DPV	0.4	61
Zn ferrite/MWCNTs/CPE	BR pH 2	DPV	0.148	This work

3.5. Repeatability, fabrication reproducibility and stability

The repeatability of measurement was performed by running 7 successive scannings for 1.64×10^{-6} mol L^{-1} HVA on the same electrode under the optimum conditions. The fabricated sensors showed acceptable repeatability with a relative standard deviation of 2.48%. Five fabricated sensors were applied for DPV determination of 1.64×10^{-6} mol L^{-1} HVA under the same conditions. The relative standard deviation of recovery of electrodes fabricated independently did not exceed the value of 1.35 %.

The constructed sensors modified with ZFO/MWCNTs/CPE showed long-term storage stability when stored at room temperature; sensors retained 95 % and 92 % of their initial peak current in 1.64×10^{-6} mol L^{-1} HVA after 10 and 20 days, respectively. Prolong storage periods may result in further diminishing of the HVA peak current which may be attributed to alteration of the nanocomposite structure after successive measurements and storage.

3.6. Interference studies

The coexisting uric acid and dopamine at high concentrations in the urine samples of neuroblastoma (NB) patients hinder the electrochemical detection of neurotransmitters in biological samples. Applying the ZFO/MWCNTs/CPE, high resolution between the HVA peak and those for UA and DA (more than 0.25 and 0.4 V between the peak potential of HVA, UA, and DA, respectively) was recorded (S8). Moreover, the peak potentials of Levodopa (L-DOPA, 20×10^{-6} mol L^{-1}), and ascorbic acid (AA, 20×10^{-6} mol L^{-1}) at pH 2 BR are far away from those of HVA (at 0.658 V).

To investigate the selectivity of the proposed protocol, the DPV graphs for 2.0×10^{-6} mol L^{-1} HVA were recorded in presence of increasing the concentration of other interfering species. The results show that the tolerance limit (±5% recovery) was about 100-fold excess of Zn^{2+}, Na^{+}, Ca^{2+}, Mg^{2+}, Cl^{-} and SO_4^{2-}, while 50-fold lysine (Lys), cysteine (Cys), L-glycine (Lgy), L-glutamic acid (Lga), tryptophan (try), folic acid (FA), valine (Val) and bovine serum albumin (BSA) and glucose (Glu) do not show a noticeable interference.

3.7. Sample analysis

As the normal level of urinary homovanillic acids ranged from 8.2 to 41.0×10^{-6} mol L^{-1} [63], the obtained sensitivity and selectivity of the fabricated sensor indicated its reliability and applicability for real sample analysis. To verify the practical applicability of the proposed analytical protocol, the fabricated ZFO/MWCNTs/CPE was applied to determine HVA in urine samples collected from healthy adult personnel. No filtration or centrifugation was required where the samples were diluted 10-fold with the buffer solution prior to electrochemical analysis. The standard addition method was adopted to verify the accuracy of the analysis. The modified sensor showed quantitation recoveries ranged from 94.66 to 101.7 % with RDS values below 5 % which were acceptable in bio sample assays (Table 2).

Table 2. Recoveries of homovanillic acid from healthy human urine samples applying ZFO/MWCNTs/CPE sensors at pH 2.0

Sample	Add ($\times 10^{-6}$ mol L^{-1})	Found ($\times 10^{-6}$ mol L^{-1})	Recovery (%)	RSD (%)
Urine	5	4.94	98.8	2.98
	10	10.17	101.7	2.05
	15	14.2	94.66	3.55
	20	19.4	97.0	2.32

4. CONCLUSION

Herein, novel carbon paste electrodes modified with Zn ferrite/MWCNTs composite were introduced as an efficient analysis protocol for submicromolar voltammetric determination of homovanillic acid for Neuroblastoma diagnosis. Modification with the ferrite nanocomposite offered electrocatalytic activity towards electrochemical oxidation of the target analyte with significant enhancement of the peak current compared with the bare electrode. Indeed, the proposed sensor showed improved selectivity towards HVA in presence of other species present in the urine samples. At the optimum conditions, the linear calibration curve was constructed in the HVA concentration ranged between 0.415 to 3.222×10^{-6} mol L^{-1} HVA with LOD value of 0.148×10^{-6} mol L^{-1}; therefore, it can be applied for the analysis of urine samples without prior pretreatment or preconcentration protocol.

CONFLICTS OF INTEREST

Authors declare they have no conflict of interest.

ACKNOWLEDGMENT

Dr. Mohamed acknowledges Taif University Researchers Supporting Project number (TURSP-2020/43). Taif University, Taif, Saudi Arabia.

SUPPLEMENTARY MATERIAL

Table S1. Average size crystallite particles, lattice parameters and inter-planar spacing of the unit cell calculated from XRD data of metals substituted ZFO NPs.

Doped ferrites	FWHM β (degree)	Inter-planar spacing d (Å)	Crystallite size D ± 1.5 (nm)	Lattice parameter a_{exp} (Å)	Lattice parameter $a_{the.}$ (Å)
FO	0.495	2.5325	10.85	8.385	8.36120
ZCFO	0.521	2.5213	11.56	8.415	8.29634
ZFO	0.623	2.5241	15.17	8.282	8.26340
ZMFO	0.445	2.5412	32.20	8.314	8.19520

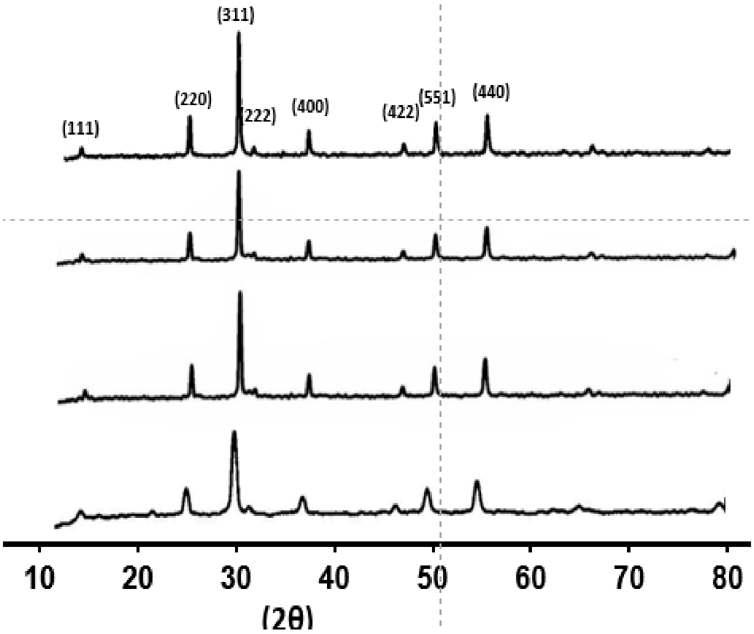

Figure S1. XRD of, a) ZFO, b) ZCFO, c) ZMFO, and d) FO ferrite NPs

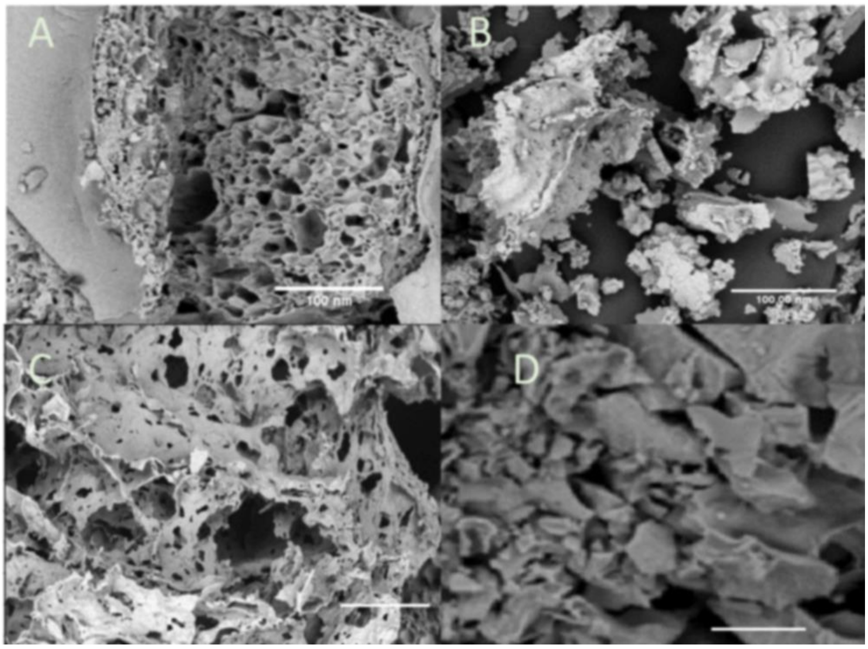

Figure S2. SEM Images of, a) ZFO, b) ZCFO, c) ZMFO, and d) FO ferrite NPs

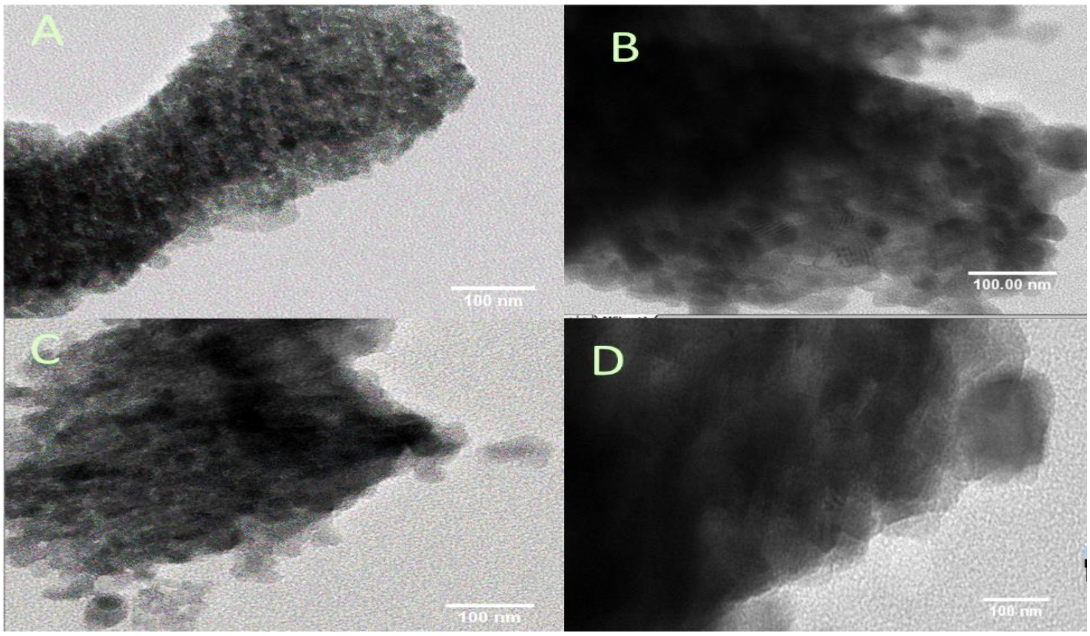

Figure S3. TEM Images a) ZFO, b) ZCFO, c) ZMFO, and d) FO ferrite NPs

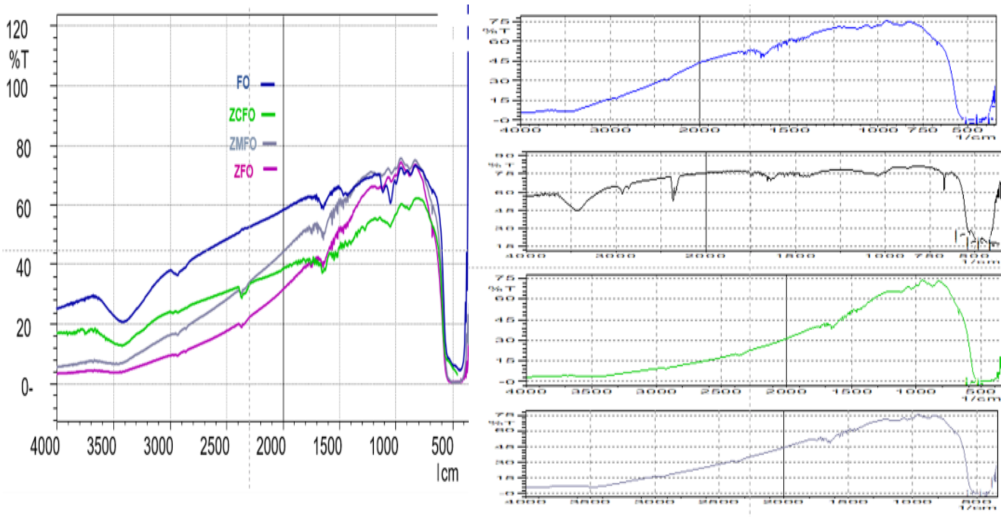

Figure S4. FTIR of, a) ZFO, b) ZCFO, c) ZMFO, and d) FO ferrite NPs

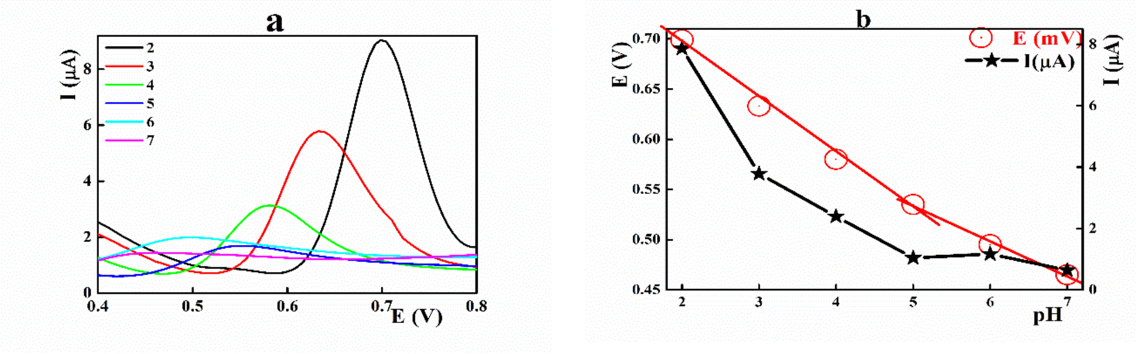

Figure S5. DP voltammograms of 2.0 μ mol HVA on CPE recorded at different pH values. Scan rate of 50 mV s^{-1} was applied.

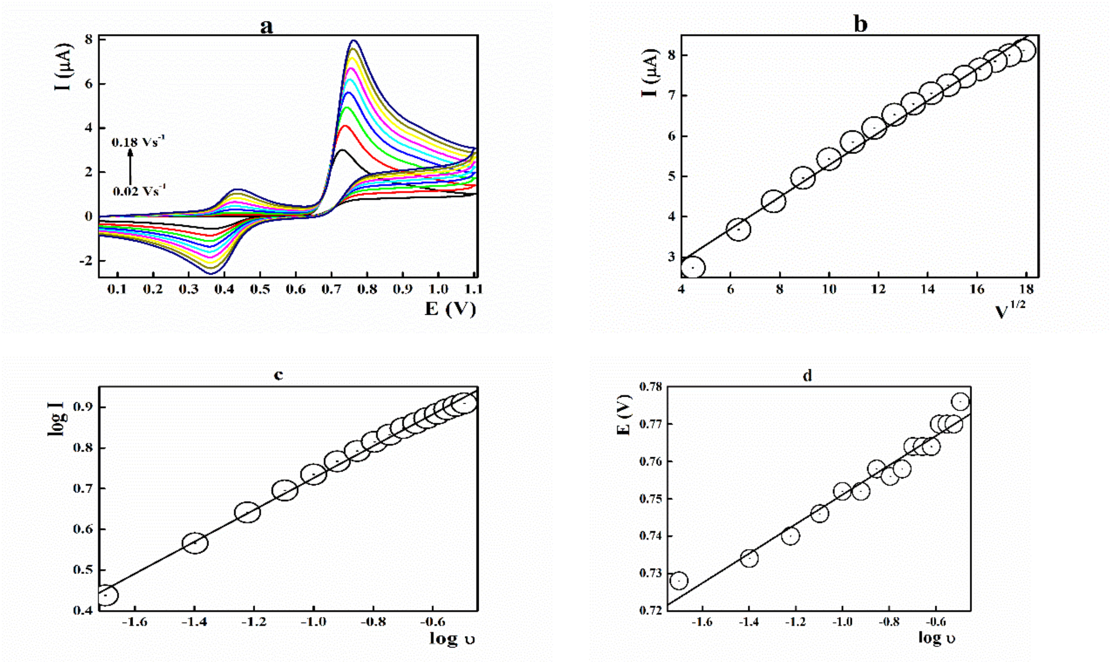

Figure S6. The influence of scan rate on the cyclic voltammetric behavior of 1.23×10^{-6} mol L^{-1} HVA on CPE at pH 2.

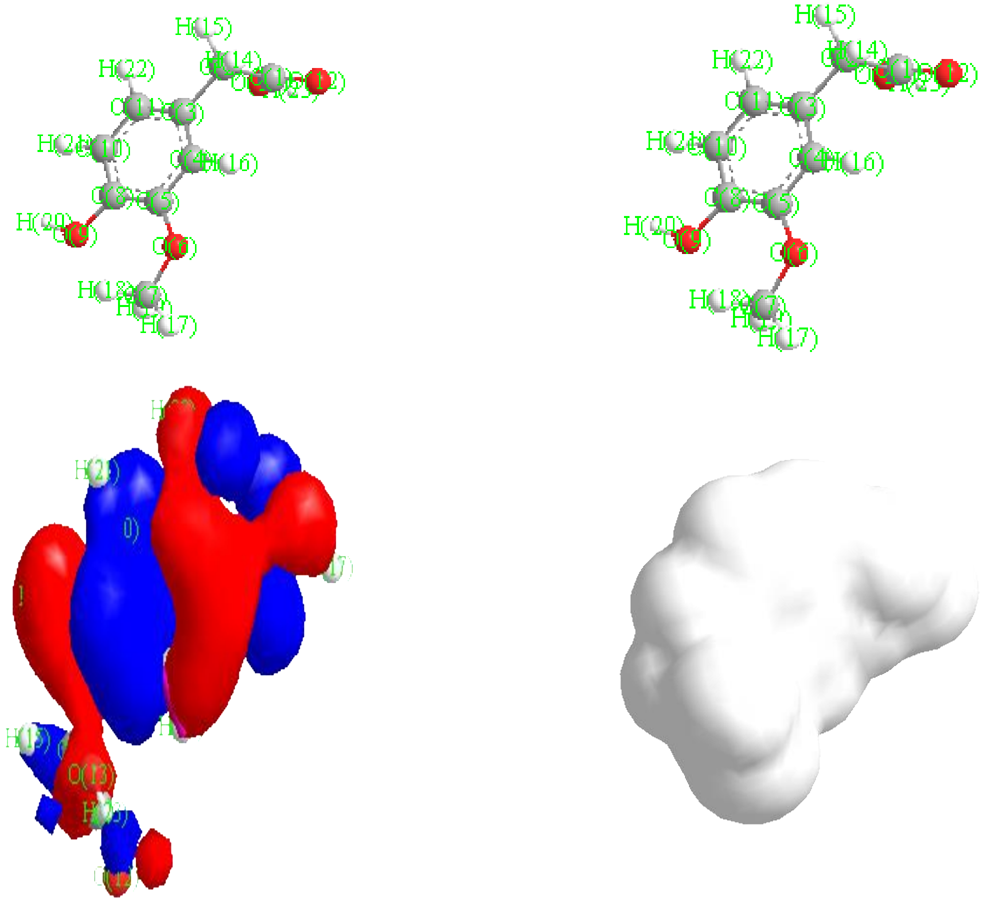

Figure S7. Molecular structure (with numbering)

Table S2: Nucleophilic, electrophilic and radical Fukui indices of HVA sites.

Atom	Atom Type (MM2)	Atom Type (MMFF94)	Charge (MMFF94)	Charge (Huckel)	Mulliken Charges (Mopac Interface)	Mopac Interface: Electrostatic Potential (Mopac Interface)
C(1)	C Carbonyl	0 CARBOXYLI	0.659	0.611802	0.681461	1.6538
C(2)	C Alkane	0 ALKYL CAR	0.2045	-0.119357	-0 [illegible]	-1.4988
C(3)	C Alkene	0 AROMATIC	-0.1435	0.0545773	-0.002469	0.91
C(4)	C Alkene	0 AROMATIC	-0.15	-0.126388	-0.258244	-0.26
C(5)	C Alkene	0 AROMATIC	0.0825	0.179531	0.176772	-0.1062
O(6)	O Enol	0 ALCOHOL O	-0.3625	-0.213074	-0.318142	-0.1403
C(7)	C Alkane	0 ALKYL CAR	0.28	0.0723101	-0.322989	-0.4528
C(8)	C Alkene	0 AROMATIC	0.0825	0.181331	0.152051	0.1537
O(9)	O Enol	0 ENOLIC OR	-0.5325	-0.274319	-0.511786	-0.4387
C(10)	C Alkene	0 AROMATIC	-0.15	-0.10501	-0.288998	-0.0034
C(11)	C Alkene	0 AROMATIC	-0.15	-0.100551	-0.20196	-0.7303
O(12)	O Carbonyl	0 CARBONYL	-0.57	-0.63644	-0.516063	-0.927
O(13)	O Carboxyl	0 ESTER OR	-0.65	-0.177877	-0.608503	-0.9693

H(14)	H	0 H ATTACH	0	0.0429616	0.240411	0.3198
H(15)	H	0 H ATTACH	0	0.050658	0.240605	0.4651
H(16)	H	0 H ATTACH	0.15	0.0222812	0.248093	0.1367
H(17)	H	0 H ATTACH	0	0.0283161	0.192418	0.2466
H(18)	H	0 H ATTACH	0	0.0249152	0.191532	0.1112
H(19)	H	0 H ATTACH	0	0.0242803	0.191463	0.251
H(20)	H Enol	0 ENOLIC OR	0.45	0.204856	0.35213	0.3588
H(21)	H	0 H ATTACH	0.15	0.0244174	0.21231	0.1464
H(22)	H	0 H ATTACH	0.15	0.0187588	0.216451	0.275
H(23)	H Carboxyl	0 HYDROXYL	0.5	0.21202	0.383638	0.4988

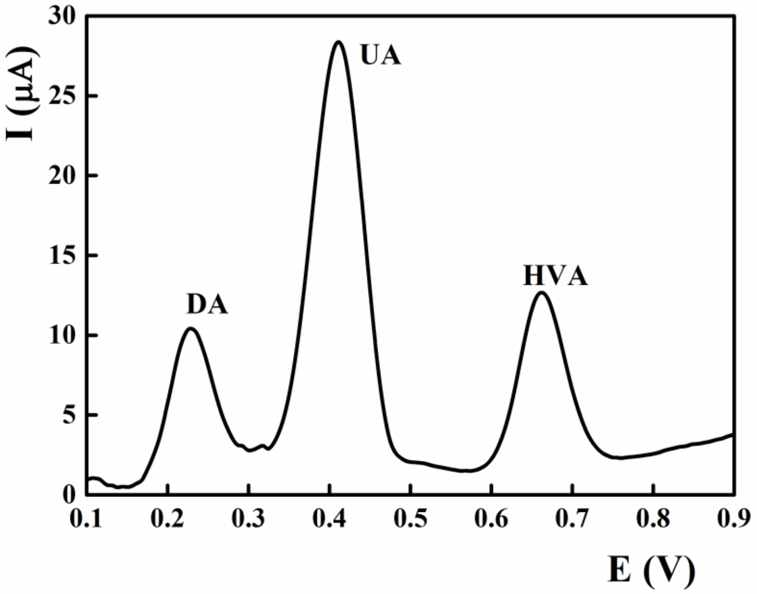

Figure S8. DPV at ZFO/MWCNTs/CPE electrode in BR, pH=2.0 containing 1.64 µ mol L^{-1} HVA in the presence of 1 µ mol L^{-1} UA and 3 µ mol L^{-1} DA. The scan rate was 0.050V.

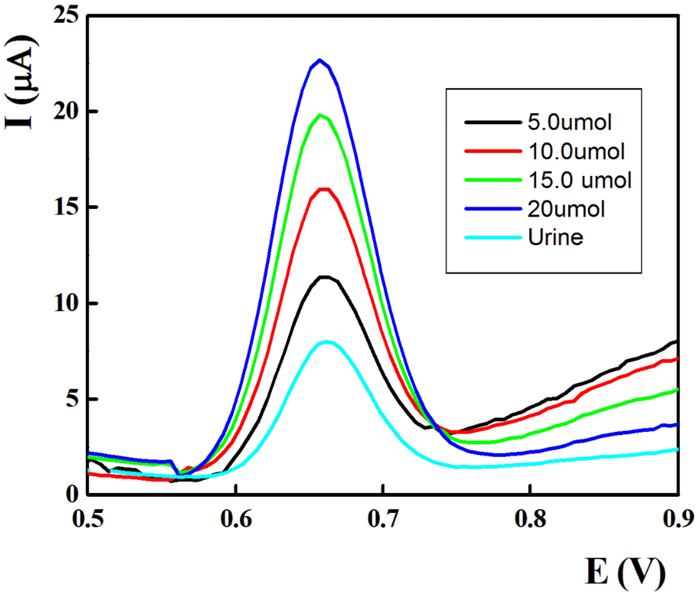

Figure S9. Standard addition method for differential pulse voltammetric determination of HVA in urine sample

References

1. G. Eisenhofer and I.J. Kopin, *Pharmacol. Rev.,* 56 (2004) 331.
2. M. Matsuo, R. Tasaki, H. Kodama and Y. Hamasaki, *J. Inherit. Metabolic Dis.*, 28 (2005) 89.
3. T. Manickum, *J. Chromatogr.* B, 877 (2009) 4140.
4. W.G. He, Y. Yan, W. Tang, R. Cai and G. Ren, *Oncotarget*, 8 (2017) 37730.
5. A. Garcıa, M. Heinänen, L.M. Jiménez and C. Barbas, *J. Chromatogr. A*, 871 (2000) 341.
6. M. Tuchman, C.L. Morris, M.L. Ramnaraine, L.D. Bowers and W. Krivit, *Pediatrics*, 75 (1985) 324.
7. S.A. Allen, S. Rednour, S. Shepard and B.B. Pond, *Biomed. Chromatogr.*, 31 (2017) e3998.
8. L. Mercolini, G. Gerra, M. Consorti, L. Somaini and M.A. Raggi, *Talanta*, 78 (2009) 150.
9. K. Uchikura, *Anal. Sci.*, 6 (1990) 351.
10. M. Tsunoda, *Anal. Bioanal. Chem.*, 386 (2006) 506.
11. G.M. Cao and T. Hoshino, *Chromatographia*, 47 (1998) 396.
12. R.T. Peaston and C. Weinkove, *Ann. Clin. Biochem.*, 41 (2004) 17.
13. Y. Zhou, H. Yan, Q. Xie, S. Huang, J. Liu, Z. Li, A. Ma and S. Yao, *Analyst*, 138 (2013) 7246.
14. J. Korf and T. Valkenburgh-Sikkema, *Clin. Chim. Acta*, 26 (1969) 301.
15. G. Fauler, H.J. Leis, E. Huber, C. Schellauf, R. Kerbl, C. Urban and H. Gleispach, *J. Mass Spectrom.*, 32 (1997) 507.
16. M. Monteleone, A. Naccarato, G. Sindona and A. Tagarelli, *Anal. Chim. Acta*, 759 (2013) 66.
17. G. Alemany, M. Akaarir, C. Rossello and A. Gamundi, *Biomed. Chromatogr.*, 10 (1996) 225.
18. F. Taran, Y. Frobert, C. Créminon, J. Grassi, D. Olichon, C. Mioskowski and P. Pradelles, *Clin. Chem.*, 43 (1997) 363.
19. F. Taran, H. Bernard, A. Valleix, C. Créminon, J. Grassi, D. Olichon, J.R. Deverre and P. Pradelles, *Clin. Chim. Acta*, 264 (1997) 177.
20. J.J. Pisano, J.R. Crout and D. Abraham, *Clin. Chim. Acta*, 7 (1962) 285.
21. X. Li, W. Jin and Q. Weng, *Anal. Chim. Acta*, 461 (2002) 123.

22. D. Flottmann, J. Hins, C. Rettenmaier, N. Schnell, Z. Kuçi, G. Merkel, G. Seitz and G. Bruchelt, *Microchim. Acta*, 154 (2006) 49.
23. D. Barh, A. Carpi, M. Verma and M. Gunduz (Eds.). Cancer biomarkers: minimal and noninvasive early diagnosis and prognosis. CRC Press, 2014.
24. S.A. Özkan, B. Uslu and H.Y. Aboul-Enein, *Crit. Rev. Anal. Chem.*, 33 (2003) 155.
25. J. Wang, *Biosens. Bioelectron.*, 21 (2006) 1887.
26. S.A. Ozkan, J.M. Kauffmann and P. Zuman, Electroanalysis in biomedical and pharmaceutical sciences: voltammetry, amperometry, biosensors, applications. Springer, 2015.
27. L. Angnes, Pharmaceuticals and personal care products. In Environmental analysis by electrochemical sensors and biosensors (pp. 881-903). Springer, New York, NY, 2015.
28. A. Makrlikova, J. Barek, V. Vyskocil and T. Navratil, *Chem. Listy*, 112 (2018) 605.
29. R. Pfeifer, P.T. Martinhon, C. Sousa, J.C. Moreira, M.A.C. Nascimento, J. Barek and V. Vyskočil, *J. Electroanal. Chem.*, 838 (2019) 129.
30. S. Hafizi, Z.L. Kruk and J.A. Stamford, *J. Electroanal. Chem.*, 283 (1990) 125.
31. M.H. Joseph, H. Hodges and J.A. Gray, Neurosci., 32 (1989) 195.
32. M.H. Joseph and A.M. Young, *J. Neurosci. Meth.*, 36 (1991) 209.
33. L.A. Mulla, J.P. Lowry, P.A. Serra and R.D. 'Neill, *Analys*t, 134 (2009) 893.
34. H. Dejmkova, H. Adamkova, J. Barek and J. Zima, *Monatsh. Chem.-Chem. Month.*, 148 (2017) 511.
35. M. Libansky, J. Zima, J. Barek and H. Dejmkova, *Monatsh. Chem.-Chem. Month*., 147 (2016) 89.
36. A. Makrlíková, E. Ktena, A. Economou, J. Fischer, T. Navrátil, J. Barek and V. Vyskočil, *Electroanal.*, 29 (2017) 146.
37. B. Fu, H. Chen, Z. Yan, Z. Zhang, J. Chen, T. Liu and K. Li, *J. Electroanal. Chem.*, 866 (2020) 114165.
38. Y. Ruan, P. Shi, Y. Lei, S. Weng, S. Li, L. Huang, X. Lin and H. Yao, *J. Electroanal. Chem.*, 848 (2019) 113267.
39. A. Hatefi-Mehrjardi, N. Ghaemi, M.A. Karimi, M. Ghasemi and S. Islami-Ramchahi, *Electroanal.*, 26 (2014) 2491.
40. S. Baluchová, J. Barek, L.I. Tomé, C.M. Brett and K. Schwarzová-Pecková, *J. Electroanal. Chem.*, 821 (2018) 22.
41. T.V. Shishkanova, G. Broncová, P. Fitl, V. Král and J. Barek, *Electroanal.*, 30 (2018) 734.
42. R. El Khamlichi, D. Bouchta, M.B. Atia, A. Attar, M. Choukairi, S. Tazi, R. Ihssane, C. Faiza, D. Khalid and R.T. Khalid, *Mater. Sci. Eng. C* 71 (2017) 870.
43. M.C. Blanco-López, M.J. Lobo-Castañón, A.M.J. Ordieres and P. Tuñón-Blanco, *Electroanal.*, 19 (2007) 207.
44. M.A. Maksoud, G.S El-Sayyad, A.H. Ashour, A.I. El-Batal, M.S. Abd-Elmonem, H.A. Hendawy, E.K. Abdel-Khalek, S. Labib, E. Abdeltwab and M.M. El-Okr, *Mater. Sci. Eng. C*, 92 (2018) 644.
45. T. Tatarchuk, M. Bououdina, W. Macyk, O. Shyichuk, N. Paliychuk, I. Yaremiy, B. Al-Najar and M. Pacia, *Nanoscale Res. Lett.*, 12 (2017) 1.
46. S.B. Mullani, A.G. Dhodamani, A. Shellikeri, N.B. Mullani, A.K. Tawade, S.N. Tayade, J. Biscay, L. Dennany and S.D. Delekar, *Sci. Rep.*, 10 (2020) 1.
47. S.B. Khan, S. Irfan and S.L. Lee, *Nanomaterials*, 9 (2019) 1024.
48. I. Svancara, K. Kalcher, A. Walcarius and K. Vytras, Electroanalysis with carbon paste electrodes. Crc Press, 2012.
49. Guideline, ICH Harmonised Tripartite. "Validation of analytical procedures: text and methodology." *Q2 (R1)* 1, no. 20 (2005) 05**.**
50. V. Jouikov and J. Simonet, Electrochemical reactions of sulfur organic compounds, Encyclopedia of electrochemistry, Vol. 8. Weinheim, Germany: Wiley-VCH Verlag GmbH & Co.; 2007. pp. 235e71.
51. A.K. Vidyadharan, J. Divya and T.E. Mary, *J. Solid State Electrochem.*, 18 (2014) 2513.

52. Z. Shahnavaz, L. Farnaz, P.M. Woi and A. Yatimah, *J. Solid State Electrochem.*, 19 (2015) 1223.
53. J. Jaime-González, E. Mazario, N. Menendez, J. Sanchez-Marcos, A. Muñoz-Bonilla and P. Herrasti, *J. Solid State Electrochem.*, 20 (2016) 1191.
54. N. Elgrishi, K.J. Rountree, B.D. McCarthy, E.S. Rountree, T.T. Eisenhart and J.L. Dempsey, *J. Chem. Educ.,* 95 (2018) 197.
55. J. Bicker, A. Fortuna, G. Alves and A. Falcao, *Anal. Chim. Acta*, 768 (2013) 12.
56. Z.H. Sheng, X.Q. Zheng, J.Y. Xu, W.J. Bao, F.B. Wang and X.H. Xia, *Biosens. Bioelectron.*, 34 (2012) 125.
57. R.S. Nicholson and I. Shain, *Anal. Chem.*, 36 (1964) 706.
58. H. Ma, N. Hu and J.F. Rusling *Langmuir*, 16 (2000) 4969.
59. S.B. Revin and S.A. John, *Anal. Meth*., 4 (2012) 348.
60. T. Selvaraju and R. Ramaraj, *Electrochim. Acta*, 52 (2007) 2998.
61. V. Hrdlička, J. Barek and T. Navrátil, *Talanta*, 221 (2021) 121594.
62. M.C. Blanco-Lopez, M.J. Lobo-Castanon, A.J. Miranda-Ordieres and P. Tunon-Blanco, *Biosens. Bioelectron.*, 18 (2003) 353.
63. H. Sirén, M. Mielonen and M. Herlevi, *J. Chromatogr. A*, 1032 (2004) 289.